CrystEngComm

PAPER

Nanocrystalline diamond microstructures from Ar/H$_2$/CH$_4$-plasma chemical vapour deposition†

I-Nan Lin,[a] **Huang-Chin Chen,**[a] **Chuang-Shern Wang,**[ab] **Yun-Rue Lee**[a] **and Chi-Young Lee**[*cd]

The incorporation of H$_2$ into Ar plasma was observed to markedly alter the microstructure of diamond films. The addition of a small percentage of H$_2$ (<1.5%) into the Ar plasma leads to the presence of stacking faults in plate-like diamond grains, the incorporation of 75% H$_2$ induces the formation of the diamond polymorph (8H). Optical emission spectroscopy indicated that addition of H$_2$ into the Ar/ CH$_4$ plasma decreased the CH/C$_2$ ratio and increased the proportion of atomic hydrogen. The small proportion of atomic hydrogen in 1.5%H$_2$–Ar plasma can only induce the formation of (111) stacking faults, resulting in scarcely distributed plate-like diamond grains. The large proportion of atomic hydrogen in 75%H$_2$–Ar plasma causes the rapid growth of diamond grains, leading to the formation of polymorphs of diamond lattices. The tuning on the microstructure of the UNCD films by incorporating either small or large amounts of H$_2$ in Ar-plasma can be attributed to the interaction of H-species with the grain boundary hydrocarbons. Such a capability opens up the potential for applications of UNCD films. Despite the complication in granular structure resulted from the CH$_4$/(Ar–H$_2$) plasma chemical vapour deposition, the formation of microstructures can be explained by the same pathway, the competition of the processes (i) formation of a hydrocarbon passivation layer and the re-activation of the hydrocarbon layer and (ii) secondary nucleation and the enlargement of diamond grains.

Introduction

Diamond films possess marvellous physical and chemical properties, such as a wide band-gap, a high acoustic wave velocity, high thermal conductivity, chemical inertness, a large electrochemical window, high mechanical strength and high biocompatibility. They have great potential for device applications. Recently, the main focus of research has been directed towards the synthesis and properties of ultra-nanocrystalline diamond (UNCD) films containing nano-sized grains,[1] as the UNCD films possess many excellent properties and several of them actually exceed those of microcrystalline diamond (MCD), containing micron-sized grains.[2] Contrary to the conventional process for synthesizing the MCD films that utilized H$_2$ plasma and requires a high substrate temperature (~900 °C), the growth of UNCD films used Ar plasma, which grew the UNCD films at very low substrate temperature.[3,4] Such a "low temperature" process is more compatible with the semiconductor device process. However, the microstructure of UNCD films, which significantly influences the physical and chemical properties needed for applications, is extremely sensitive to the growth parameters, especially the constituents of the plasma.[5–9] MCD films grown in CH$_4$/H$_2$ plasma usually contain large faceted grains, whereas UNCD films grown in CH$_4$/Ar plasma usually consist of ultra-small grains of equi-axed geometry. It has been proposed that C$_2$-dimers are the growing species for the ultra-small sized diamond grains.[8] However, recent studies indicated that the species adjacent to the substrates are actually far more complicated.[10–12] It contains CH$_3$$^+$, CH$_2$$^+$, CH$^+$ and C$_1$ species. While such a model provided a better understanding of the authentic species for growing the diamond, how the microstructure of the diamond changes with the constituents in the plasma is still not well explained.

Jiao *et al.*[5] proposed that atomic hydrogen plays a critical role in determining the nucleation interface between the UNCD films and the Si substrates, whereas Birrell *et al.*[6] observed that addition of hydrogen in the gas phase results in a competitive growth between MCD and UNCD grains, rather than a simple increase in the grain size of UNCD. However, how the presence of hydrogen influences the growth behaviour of UNCD films has still not been addressed. It is only recently that Wang *et al.*[12]

a Department of Physics, Tamkang University, Tamsui, 25137, Taiwan, R. O. C

b Technology and Science Institute of Northern Taiwan, Beitou, 11202 Taipei, Taiwan, R.O.C

c Department of Materials Science and Engineering, National Tsing Hua University, Hsinchu, Taiwan, 30013, R. O. C. E-mail: cylee@mx.nthu. edu.tw

d Center for Nanotechnology, Materials Science, and Microsystems, National Tsing Hua University, Hsinchu, Taiwan, 30013, R. O. C

† Electronic supplementary information (ESI) available: polymorphs of tetrahedral bonded carbons; TEM microstructure of UNCD$_{10}$ films. See DOI: 10.1039/c1ce05517h

proposed that the addition of a small percentage of H_2 into Ar-plasma induced the anisotropic growth of the diamond grains. While such an observation explains the formation of the plate-like diamond grains among the UNCD grains very well, the evolution of granular structure was not elucidated with the plasma containing a large proportion of H_2.

In the present study, we extent the range of investigation, that is, we synthesized diamond films using a microwave plasma enhanced chemical vapour deposition (CVD) process with a plasma containing an excess CH_4/H_2 ratio with a small percentage of Ar. Transmission electron microscopy (TEM) was used to investigate the detailed microstructure of the diamond. We observed that the diamond synthesized in such a H_2-riched $CH_4/(Ar–H_2)$ plasma contained a large proportion of hexagonal diamond with the polymorph cubic diamond. Based on these observations, a unified model for the formation of the granular structure of diamond with respect to the constituents of the plasma is proposed.

Experimental

N-type mirror polished Si (100) substrates were used to grow the diamond film. The substrates were first ultrasonically cleaned with acetone and then dipped in HF for 1 min to remove any surface contamination and native oxides. The substrates were ultrasonicated in a solution containing a mixture of diamond powders (30 nm) and Ti powders (325 nm) in methanol to facilitate the nucleation process. The substrates were again ultrasonically cleaned in deionized water to remove diamond particles, which were possibly adhered on the substrates, and then dried by blowing over with nitrogen gas. The diamond films were grown by microwave plasma CVD process using the setup from IPLAS (Innovative Plasma Systems GmbH, Cyrannus) for 3 h, with a microwave power (2.45 GHz) of 1200 W and a chamber pressure of 100 torr in $(Ar–x\%H_2) = 99$ sccm and $CH_4 = 1$ sccm gas mixture. The diamond films were named according to the size of grains resulted. Those grown with a large proportion of H_2 ($x = 10, 40$ and 75%) were designated as $UNCD_{10}$, NCD_{40} and MCD_{75}, respectively, whereas those grown with small proportion of H_2 ($x = 0\%$ or 1.5%) were designated as $UNCD_{00}$ or $UNCD_{01}$, respectively. No external heater was used to heat the substrate and the substrate temperature was estimated to be in the range of 460–595 °C due to plasma heating.

The surface morphologies and the microstructure of the diamond films were examined by FE-SEM (JEOL JSM-6500F) and TEM (JEOL 2100), respectively. The crystalline quality of the deposited diamond films was characterized by Raman spectroscopy (Renishaw) using 514 nm laser beams and near edge X-ray absorption fine structure spectroscopy (NEXAFS).

Results and discussion

The granular structure of the diamond films is very sensitive to the constituents of the plasma. Contrary to the large faceted diamond grains for the microcrystalline diamond (MCD) films obtained in CH_4/H_2-plasma (not shown), ultra-nanocrystalline diamond (UNCD) films grown in CH_4/Ar-plasma contain extremely small sized grains with spherical morphology. Fig. 1a
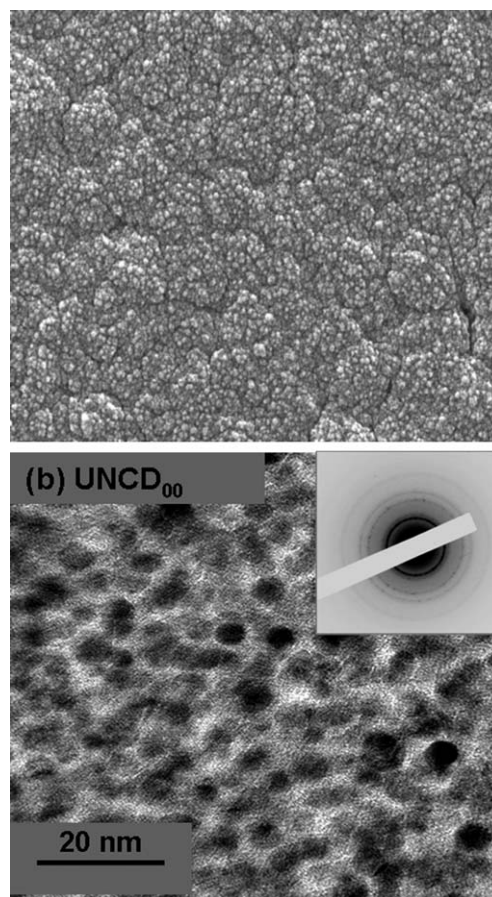

Fig. 1 The (a) SEM morphology and (b) TEM microstructure for the $UNCD_{00}$ films that were grown in CH_4/Ar plasma without the addition of H_2.

shows that the $UNCD_{00}$ films grown in $CH_4(1\%)/Ar(99\%)$ plasma possess fine grain morphology with a very smooth surface. The TEM micrograph in Fig. 1b and the selected area electron diffraction (SAED) pattern in the inset reveal that the grains contained in these films are actually diamond with very small sized ($\sim$5 nm) and are of spherical geometry, separated by amorphous grain boundaries about 1–2 nm in thickness.

The addition of H_2 into CH_4/Ar-plasma or the incorporation of Ar into CH_4/H_2-plasma markedly affects the microstructure of the diamond films. SEM examination shows that the Ar-rich plasma (1.5% or 10.0% H_2) results in an ultra-small granular structure with an extremely smooth surface ($\sim$30 nm rms, Fig. 2a and 2b), the H_2-rich plasma (40% or 75% H_2) leads to a cauliflower-like microstructure with a rough surface (Fig. 2c and 2d). TEM microstructural analyses further indicate that even a small amount of H_2 (1.5%) added into the CH_4/Ar plasma profoundly alters the morphology of the grains. The granular structure changes from a spherical appearance for 0% H_2 films ($UNCD_{00}$, Fig. 1b) to an acicular one for 1.5% H_2 films ($UNCD_{01}$, Fig. 3a). Larger amounts of H_2 ($\sim$10%) incorporated in the CH_4/Ar-plasma increase the number density of the acicular grains, which intruded on one another, forming dendrite ($UNCD_{10}$, Fig. 3b). A further increase in H_2-content increases the size of the dendrites, which finally agglomerates into large aggregates of equi-axed
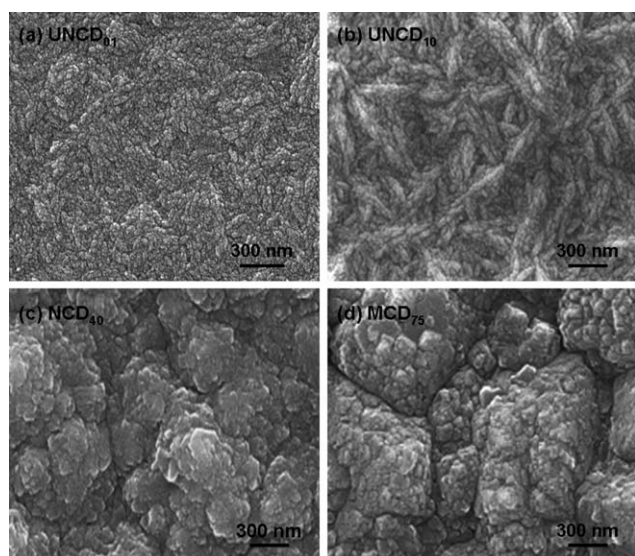
Fig. 2 SEM micrographs for the diamond films grown in Ar–x%H$_2$, where x = (a) 0% (UNCD$_{00}$), (b) 1.5% (UNCD$_{01}$), (c) 10% (UNCD$_{10}$), (d) 40% (NCD$_{40}$) and (e) 75% (MCD$_{75}$).
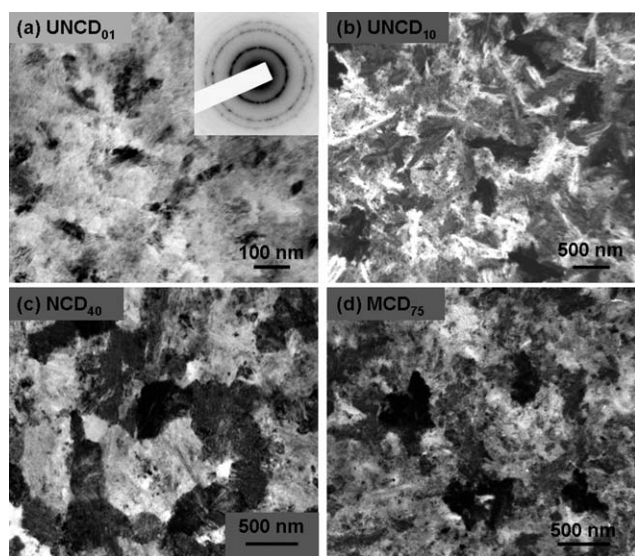
Fig. 3 TEM micrographs for the diamond films grown in Ar–x%H$_2$ plasma, where x = (a) 0% (UNCD$_{00}$), (b) 1.5% (UNCD$_{01}$), (c) 10% (UNCD$_{10}$), (d) 40% (NCD$_{40}$) and (e) 75% (MCD$_{75}$).

geometry (NCD$_{40}$, Fig. 3c and MCD$_{75}$, Fig. 3d). However, the spherical aggregates in MCD films are much larger in size (∼hundreds of nano-meters), compared with the ultra-small equi-axed grains in UNCD$_{01}$ films (∼5–10 nm).

Visible Raman spectroscopy (514 nm) shown in Fig. 4a reveals that the films grown in Ar-rich plasma (with 0–10% H$_2$) posses the characteristics of ultra-nanocrystalline diamonds, *viz.* they contain ν_1- and ν_2-resonance peaks at 1140 and 1480 cm^{-1}, respectively, representing grain boundary sp^2-bondings, presumable transpoly-acetylene[13,14] and D- and G-resonance peaks at 1380 and 1580 cm^{-1}, representing disordered and graphitic carbons, respectively.[15,16] In contrast, the films grown in 75% H$_2$ plasma posses the characteristics of microcrystalline
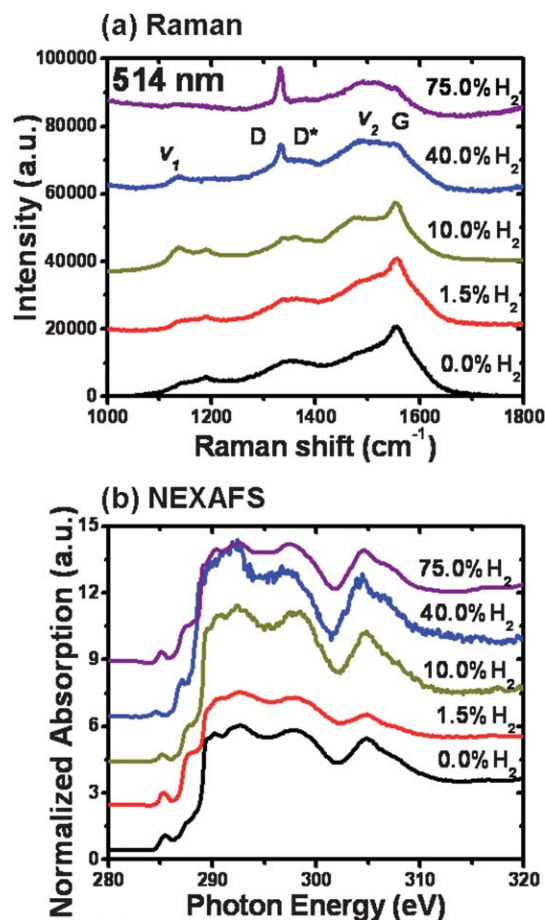
Fig. 4 (a) Raman spectroscopy (514 nm) and (b) near edge X-ray absorption fine structure (NEXAFS) for the diamond films grown in Ar–x%H$_2$, where x = 0% (UNCD$_{00}$), 1.5% (UNCD$_{01}$), 10% (UNCD$_{10}$), 40% (NCD$_{40}$) and 75% (MCD$_{75}$).

diamonds, *viz.* they contain D resonance peaks at 1320 cm^{-1}, the typical resonance peak for sp^3-bonds. The films synthesized in 40% H$_2$ plasma contain both the D-band resonance peak and small ν_1, ν_2, D* and G resonance peaks, indicating the presence of some proportion of ultra-small diamond grains co-existing with the large ones in these films. The relative intensity of the sp^3-bonded peak (1320 cm^{-1}) increases with the proportion of H$_2$ added into the plasma. The characteristics of these Raman spectra, deconvoluted using the Lorentzian distribution function, are shown in Table 1 to facilitate the comparison. Since visible Raman is more sensitive to sp^2-bonding than sp^3-bonding, it is difficult to quantitatively analyze the sp^3-bonding characteristics for these materials, and NEXAFS in synchrotron radiation is thus examined. Fig. 4b illustrates that the spectra of the films are dominated by an abrupt rise near 289.7 eV (the σ*-band) and a large dip near 305 eV, indicating that the films mainly contain sp^3-bonds.[17,18] The peak near 285.4 eV (π-band) is small for all spectra, inferring that the content of sp^2-bonded carbons is of a very small proportion, even for UNCD$_{00}$ films grown in CH$_4$/Ar plasma. Notably, all the NEXAFS contain a small jump near 288.5 eV, which corresponds to C–H bonds. Such an observation is in accordance with the proposed grain boundary phase, *i.e.*, *trans*-poly-acetylene.

Table 1 The characteristics of Raman spectra deconvoluted using the Lorentzian distribution function

Samples (%H$_2$)	ν_1 (1150 cm^{-1})		D (1332 cm^{-1})		D* 1350 (cm^{-1})		ν_2 (1480 cm^{-1})		G (1580 cm^{-1})	
	Peak	FWHM	Peak	FWHM	Peak	FWHM	Peak	FWHM	Peak	FWHM
0.0%	1145.3	29.64	—	—	1350.7	143.49	1485.9	100.81	1558	67.59
1.5%	1176.9	84.56	—	—	1348.7	128.66	1487.4	125.60	1559.5	74.83
10.0%	1136.4	36.01	—	—	1346.1	112.14	1477.8	113.71	1556.6	63.06
40.0%	1135.6	33.19	1333.4	144.39	1349.2	144.39	1486.1	113.83	1556.1	77.31
75.0%	1155.8	124.61	1332.2	11.278	1389.4	163.58	1493.4	88.35	1548.1	47.45

To understand how the incorporation of Ar into CH$_4$/H$_2$-plasma induces the dramatic change in the microstructure of UNCD films, the detailed microstructures of MCD$_{75}$ films grown in 75.0%H$_2$–25%Ar plasma were investigated. It should be remembered that, for the MCD$_{75}$ films, large clusters with irregular geometry (∼200 nm) are uniformly distributed over the films (*cf.* Fig. 3d). Fig. 5a shows a TEM micrograph of a typical large cluster in the films. The granular structure is very complicated. The structural image of the regions 1 and 2 designated in Fig. 5a is shown in Fig. 5b and 5d, respectively, to illustrate that the cluster contains a large proportion of planar defects. Fig. 5b show that, in region 1 of MCD$_{75}$, the area A is featureless, whereas the area B contains parallel fringes with irregular spacing, implying that area A contains essentially no defects and area B contains a large proportion of defects. The Fourier transformed (FT) diffractograms of the corresponding areas are shown as FT$_a$ and FT$_b$ in Fig. 5c, inferring that these regions belongs to the same grains, near the 0$\bar{1}$1 zone axis. Again, FT$_a$ contains no streak, indicating that area A is essentially defectless. Only in FT$_b$ are there streaks lying along the [111] direction associated with each diffraction spot of FT$_b$, implying that the parallel fringes in area B are an edge-on image of (111) plate-like defects, most probably stacking faults.

In addition to the stacking faults with plate-like parallel fringes (the edge-on image of the stacking faults), there also exist other form of planar defects of similar appearance in MCD$_{75}$ films. Fig. 5d shows that, in region 2 of the MCD$_{75}$ films, areas C and D contain parallel fringes that are equally spaced and are long-range ordered. The parallel fringes in areas C and D are oriented in different directions. The nature of these planar defects will be discussed shortly. Area E possesses a structure image similar to that of area A in Fig. 5b, except that this region contains a row of defects (arrowed). The FT image of area E (FT$_e$, Fig. 5c) indicates that region 2 is also the 3C lattices in the 0$\bar{1}$1 zone-axis, *i.e.*, it is oriented in the same direction as region 1. Detail analysis on the band running across the center of the structure images indicates that it is a stacking fault arranged in an ABABAB sequence, located in the matrix of lattices with ABCABC tacking sequences. It should be noted that all the areas designated in regions 1 and 2 belongs to the same grains and there is no clear boundary between them. Moreover, the adjacent regions are also composed of large diamond grains, but are oriented in a non-diffracting condition and are thus not showing contrast. Fig. 6a and 6b are, respectively, the enlarged structural images corresponding to the planar defects with widely spaced parallel fringes, *i.e.*, the areas C and D in Fig. 5d. These figures show that the lattices in the two images are oriented in different directions

and are totally different in the FT diffractograms (Fig. 6c). These diffractograms show some interesting features, *viz.* a systematic row of spots, which look like super-lattice diffraction spots. There are no streaks associated with these diffraction spots. Detail analysis using computer simulation (JEMS code, Joel) indicates that the structure images in Fig. 6a and 6b are 8H hexagonal lattices oriented on the 2$\bar{1}$1$\bar{0}$ zone axis. The detail analysis for these planar defects will be discussed in the Electronic Supplementary Information†. It should be noted that the 8H is one of the possible polymorphs of diamonds with a hexagonal structure. There are also other forms of hexagonal diamond with A, B, and C lattice planes arranged in different sequences, which contain 2H, 4H, 6H, 8H, 15R and 21R polymorphs (designated as nH).

Since the nH-lattices were defects induced during the growth of 3C-diamond materials, the formation of nH hexagonal lattices must be initiated by the misplacement of certain (111) lattice planes. Therefore, the (0001)$_{nH}$ planes of the nH-lattices must lie parallel with the ($\bar{1}$11) plane of 3C-lattices, with the [2$\bar{1}\bar{1}$0]$_{nH}$ direction of hexagonal lattices (nH) oriented parallel with the [20$\bar{2}$]$_C$ direction of the cubic lattices (3C), as schematically shown in Fig. 7a. In other words, when the electron beams were incident along the [20$\bar{2}$]$_C$ zone axis of the cubic lattices, they were also incident along the [2$\bar{1}\bar{1}$0]$_{nH}$ zone axis of the hexagonal lattices, with the [0001]$_{nH}$ g-vector lying in parallel with the <111>$_{3C}$ one, as shown in Fig. 7b. Therefore, there are two possibilities for the [0001]$_{nH}$ g-vector to orient with respect to the 3C reciprocal lattices, *viz.* [111]$_{3C}$ or [1$\bar{1}$1]$_{3C}$, shown as the schematics in Fig. 7b. Therefore, there are two variances by which the parallel fringes on (0001)$_{nH}$-lattices planes can be arranged with respect to the (111)$_{3C}$-lattices. Such an argument accounts for the simultaneous occurrence of two kind of planar defects observed in Fig. 5d, *i.e.*, areas C and D. Notably, the (111) stacking faults and nH isomorphism are the common structural defects in diamond materials grown in (75%H$_2$–25%Ar)-plasma.

To investigate how the complicated microstructure for MCD$_{75}$ films resulted, the detailed microstructure of 1.5% H$_2$–UNCD films (UNCD$_{01}$) was examined in detail. Fig. 8a shows the enlarged micrograph of a typical acicular grain in UNCD$_{01}$ films. Again, the adjacent regions are also diamond grains of a similar size, but are oriented in a non-diffracting direction and are thus showing no contrast. The SAED shown as an inset in Fig. 8a indicates that the aggregate shown in Fig. 8a is of diamond structure oriented near to the 01$\bar{1}$ zone axis. The streaks (rel-rods) oriented in the <111> direction are associated with each major diffraction spot, revealing the presence of (111) planar defects. The detailed structure of the defects is illustrated in the
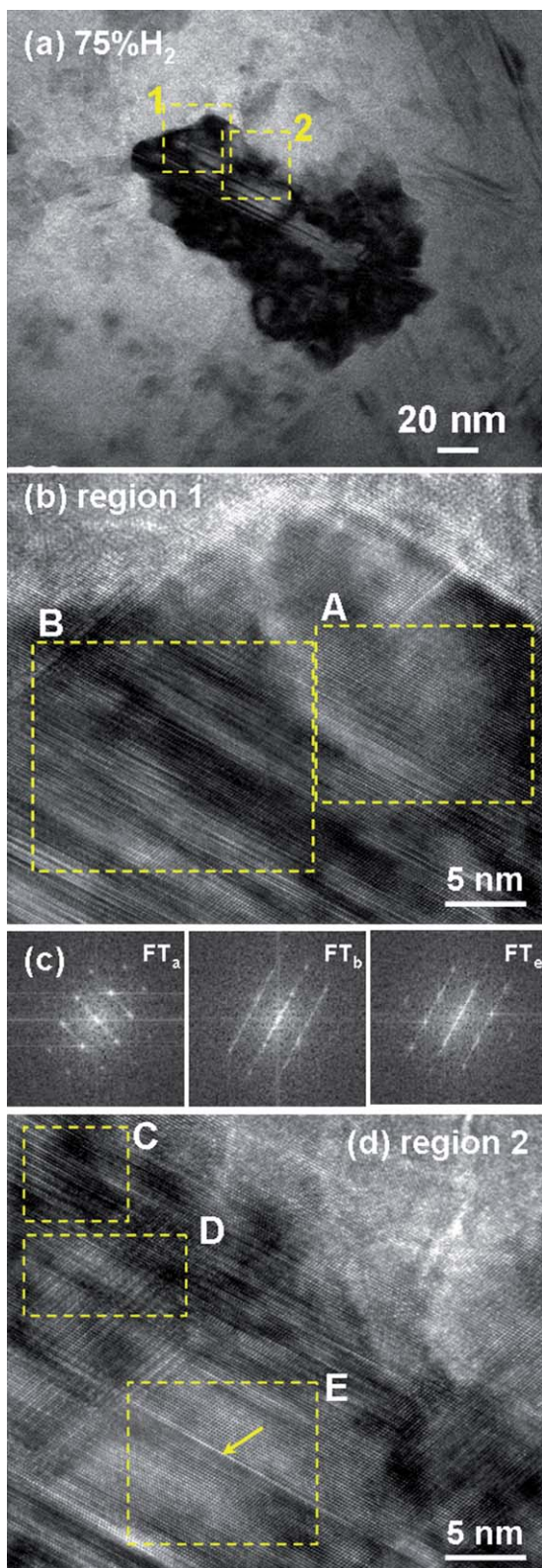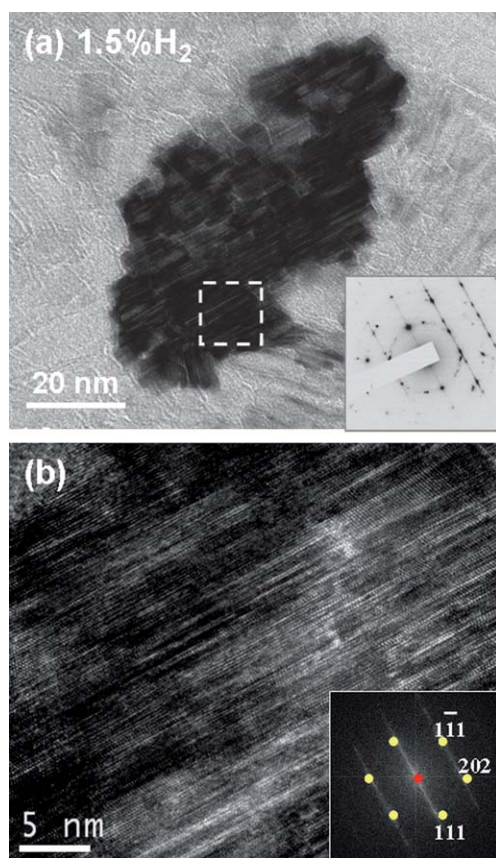
Fig. 5 TEM micrographs for the diamond films grown in 25%Ar–75% H_2 plasma (a) bright field image and structure image of (b) region 1 and (d) region 2; (c) the Fourier-transformed diffractograms of the designated regions.
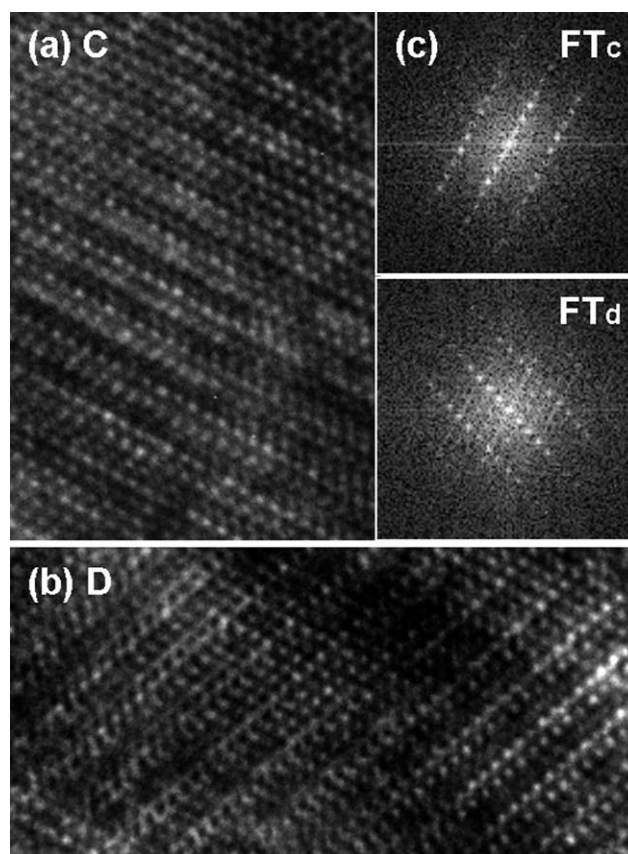
Fig. 6 The structure images of the regions designated in Fig. 5c: (a) the structure image corresponding to area C and (b) the structure image corresponding to area D; (c) the Fourier-transformed diffractograms of the corresponding structure images.
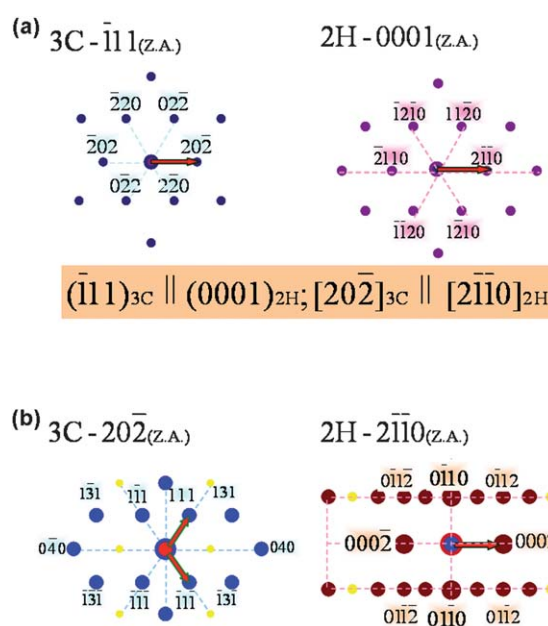

Fig. 7 The schematics of the diffraction patterns for (a) 3C-cubic lattices along the 111 zone axis and nH-hexagonal lattices along the 0001 zone-axis and for (b) 3C-cubic lattices along the 202 zone axis and nH-hexagonal lattices along the $2\bar{1}\bar{1}0$ zone-axis.

Fig. 8 TEM micrographs for the diamond films grown in Ar–1.5%H₂ plasma (a) a bright field image, with inset showing the corresponding SAED, and (b) the structure of the region designated in (a), with the inset showing the Fourier-transformed diffractogram of the structure image.

high resolution structure images (Fig. 8b), which correspond to the region designated in Fig. 8a. The associated FT diffracto-grams (inset, Fig. 8b) confirm that the parallel fringes are edged on (111) planar defects rather than needle-like precipitates, as there are -rods lying in the <111> direction. It should be noted that such a microstructure is very similar to the one shown in region B of the MCD_{75} films (cf. Fig. 5b), except that the aggregates in MCD_{75} films (Fig. 5b) are about 200 nm in size, whereas those in $UNCD_{01}$ films are relatively small in size ($\sim$30 $\times$ 70 nm) and only scarcely distributed in the films. These results implied that the microstructures of these two materials are formed by a similar process.

The optical emission spectroscopy (OES) of the plasma was investigated to explore how the addition of H₂ into the plasma affects the microstructure of the UNCD films. Fig. 9a shows the typical OES spectra for the CH₄/Ar/H₂ plasma. This figure indicates that all of the CH₄/Ar/H₂ plasma is predominated with the Swan-band near 516 nm[19,20] with a very small amount of CH species (431 nm). Moreover, atomic hydrogen species were induced for the CH₄/Ar plasma containing large proportion of H₂ (e.g. curves III–V). The intensity of the H_α (656 nm) and H_β (486 nm) lines[21,22] and the H_β/H_α intensity ratio increase with the H₂ content in the plasma (open symbols, Fig. 7b), implying that the electron temperature (T_e) of the plasma increases with the H₂ content. The electron temperature can be estimated using the Boltzmann plots,[23,24] viz.
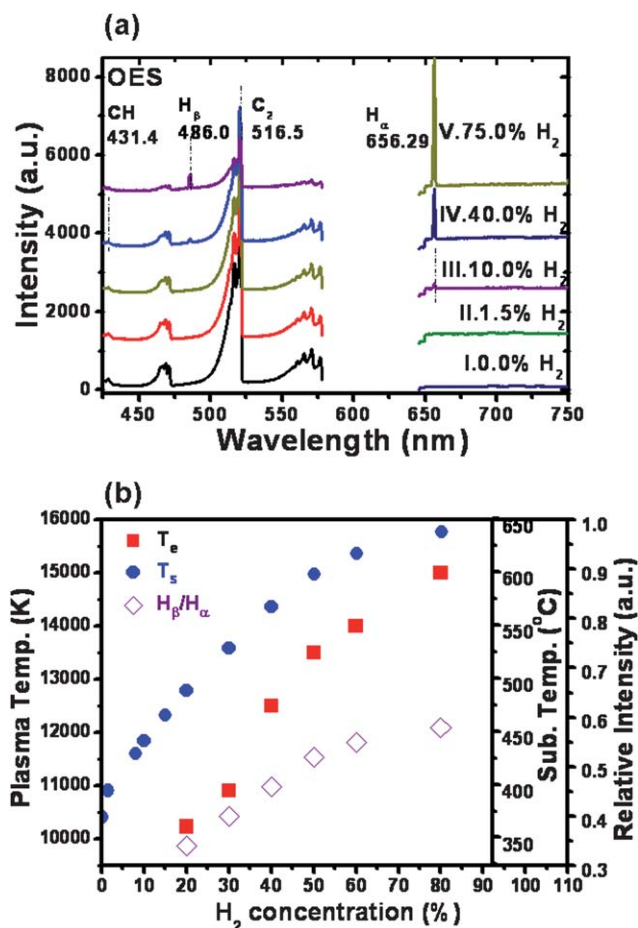
Fig. 9 (a) The optical emission spectra for the diamond films grown in Ar-x%H₂, where x = 0% (UNCD₀₀), 1.5% (UNCD₀₁), 10% (UNCD₁₀), 40% (NCD₄₀), 75% (MCD₇₅) and 100% and (b) the variation of H_β/H_α ratio and electron temperature with H₂-content in the plasma.

$$\frac{I_{ji}}{I_{kj}} = \frac{\lambda_{ki}A_{ji}g_j}{\lambda_{ji}A_{kj}g_k}\exp\left(\frac{E_k - E_j}{k_B T_{ex}}\right), \qquad (1)$$

where I_{ji} and λ_{ji} are the intensity and wavelength of the spectral line corresponding to the transition between E_j and E_i energy level; k_B is the Boltzmann constant; A_{ji} and g_j is the corresponding Einstein transition probability and statistical weight, which can be acquired from the literature.[25] Fig. 9b (solid symbols) illustrates that the electron temperature (T_e) of the plasma increases monotonically with the proportion of H₂-species incorporated. It should be noted that the data corresponding to plasma with other Ar/H₂ ratio were included in Fig. 9b to facilitate the comparison. The significance of such an observation on the formation of diamond granular structure pathway will be discussed shortly.

Discussion

The intriguing feature of the microstructure of UNCD₀₀ films is that the grain size distribution is extremely uniform ($\sim$5 nm). Moreover, unlike the commonly observed phenomenon that the grain size increases with the film thickness for MCD films, the grains in UNCD films remained at a small size, even when

the films grew to tens of microns in thickness. The narrow distribution in grain size has also been observed for nano-sized diamond particulates (~5 nm) prepared by a detonation process,[26] the detonated diamond particulates (DDP). The structure of DDP has been proposed to consist of a sp^3 hybridized carbon core and a fullerene-like sp^2 carbon shell.[27] A similar core–shell like structure is expected for the grains in UNCD films, viz. the grain interior contains sp^3-hybridized carbons and the grain boundaries contain sp^2-carbons. Such a core–shell like structure has also been proposed by first principles calculation.[28] Although the selected area electron diffraction (SAED) shown as an inset in Fig. 1b clearly indicates the crystalline structure nature (3C diamond structure) for the central part of the diamond grains, the TEM micrograph in Fig. 1b cannot clearly delineate the grain boundaries and the grain boundary structure. Such a phenomenon is very much different from the granular structure of the conventional poly-crystalline materials. The probable reason for the difficulty in imaging the grain boundaries is that the ultra-small grains might be encapsulated by hydrocarbons,[13] which are amorphous and do not diffract the electrons.

Recent studies[9–11] indicated that the species adjacent to the substrates actually contain CH_3^+, CH_2^+, CH^+ and C_1 species, rather than the C_2 species proposed earlier.[8] While the authentic growing species for the formation of UNCD grains are still in debate, what is clear is that the ultra-small-grain granular structure for the UNCD films can be formed only when there occur abundant secondary nucleation processes. Apparently, there must be some species, which adhere with the newly formed diamond clusters, that hinder the growth of diamond, such that the "active carbon-containing species" can only re-nucleate to form new diamond clusters. It is quite reasonable to assume that the passivation layer adhered on the newly formed diamond clusters is similar to the sp^2 carbon shell encapsulating the DDP particulates, viz. the passivation layer contains hydrocarbon, probably trans-poly-acetylene. The atomic hydrogen induced in the CH_4/(Ar–H_2) plasma will either (i) attach the dangling bonds on the diamond clusters or (ii) react with the previously formed sp^2 carbon shell on the surface of nano-sized diamond clusters to form sp^3-bonds. Both processes result in active sites on diamond clusters that are readily attacked by the active carbon species in the plasma, which leads to the grain growth.

In addition, a large proportion of the hydrogen species contained in the plasma not only induces more abundant atomic hydrogen but also increases the kinetic energy (higher plasma temperature) of the atomic hydrogen. Both factors enhanced the etching of adhered hydrocarbons and re-activate the sp^2 carbon shell. A separate investigation (not shown) reveals that the growth of grains can be induced not only by the addition of H_2 into a CH_4/Ar plasma, but also by increasing the substrate temperature when the films were grown in a CH_4/Ar plasma. It seems that the adherence and re-activation of hydrocarbons are the most plausible reasons for the induction of the grain growth process in H_2-incorporated CH_4/Ar plasma.

In low H_2 content CH_4/Ar plasma atmosphere, only the high surface energy (γ) sites were preferentially activated. Therefore, the diamond grains grew anisotropically, resulting in the formation of diamond flakes with a large proportion of stacking faults lying on (111) lattices. When a high concentration of H_2 (~100%) was incorporated into the plasma, the atomic hydrogen was sufficiently abundant and active enough to almost instantaneously activate all the hydrocarbons adhered on the surface of the diamonds. Such a process allows the active carbon-containing species to isotropically attach onto the surface of the diamonds, enlarging the diamond grains when they grew columnar-wise to form a faceted geometry. The unique faceted granular structure is presumably formed due to the different surface energy (γ) for each lattice plane.

Optical emission spectroscopy (Fig. 9a) indicates that the plasma used for growing MCD_{75} films contains "active carbon-containing species", hydrocarbon forming species, CH, C_2, and hydrocarbon activation species, H_α and H_β. The formation of MCD_{75} films is presumed to be achieved by an active carbon process and an atomic hydrogen re-activation process. However, as the proportion of atomic hydrogen is lower in the MCD_{75} growth plasma atmosphere than in 100%H_2 plasma, only a proportion of the encapsulating hydrocarbons on the diamond cluster surface can be activated. The residual hydrocarbons induced the formation of the planar defects, stacking faults and the hexagonal polymorph of diamond. On the other hand, the larger grain size in MCD_{75} films than $UNCD_{01}$ films is due to more abundant atomic hydrogen induced in this plasma atmosphere. Moreover, the presence of a large proportion of the active carbon-containing species in the 75.0%H_2–CH_4/Ar plasma, the secondary nucleation can't be ruled out either. The nano-sized grains will grow larger via an Ostwald-Ripening process. The columnar growth and Ostwald-Ripening processes occur simultaneously, resulting in extremely complicated microstructures for the MCD_{75} films. Nevertheless, the granular structure was formed by similar sequences: (i) the encapsulation of newly formed diamond clusters by hydrocarbon, (ii) secondary nucleation, (iii) re-activation of hydrocarbon by atomic hydrogen in the plasma and (iv) enlargement of diamond grains via the attachment of active carbon species in the plasma. The final microstructure is the result of the competition between these processing steps.

Conclusion

Incorporation of a large proportion of H_2 species (75%) into the CH_4/Ar plasma was observed to markedly alter the microstructure of diamond films. Optical emission spectra indicated that the addition of H_2 into the Ar/CH_4 plasma leads to the decrease in CH-species and an increase in atomic hydrogen species, relative to the C_2-species. The atomic hydrogen produced in the H_2-containing plasma can partially activate the hydrocarbons (trans-poly-acetylene) adhered onto the diamond clusters such that the active carbon-containing species in the plasma can anisotropically attach onto the diamond surface. However, the proportion of the activity of atomic hydrogen will be reduced due to the presence of 25% Ar, as compared with those in CH_4/H_2 plasma. The atomic hydrogen incompletely re-activated the encapsulating hydrocarbons, resulting in the presence of planar defects in the diamond grains. The possible planar defects include stacking faults and isomorphism of diamonds, such as nH-diamonds. The effect on the microstructure of the UNCD films is the result of the following competing processes: (i) enlargement of the

diamond grains, (ii) formation of a hydrocarbon passivation layer, (iii) secondary nucleation, and (iv) re-activation of hydrocarbons.

Acknowledgements

Notes and references

1 D. M. Gruen, *Annu. Rev. Mater. Sci.*, 1999, **29**, 211.
2 J. A. Carlisle and O. Auciello, *Electrochem. Soc. Interface*, 2003, **12** (1), 28.
3 X. Xiao, J. Birrell, J. E. Gerbi, O. Auciello and J. A. Carlisle, *J. Appl. Phys.*, 2004, **96**, 2232.
4 D. Pradhan, Y. C. Lee, C. W. Pao, W. F. Pong and I. N. Lin, *Diamond Relat. Mater.*, 2006, **15**, 2001.
5 A. Jiao, A. Sumant, M. A. Kirk, D. M. Gruen, A. R. Krauss and O. Auciello, *J. Appl. Phys.*, 2001, **90**, 118.
6 J. Birrel, J. E. Gerbi, O. Auciello and J. A. Carlisle, *J. Phys.: Condens. Matter*, 2006, **18**, S1771.
7 T. S. Yang, J. Y. Lai, C. L. Chen and M. S. Wong, *Diamond Relat. Mater.*, 2001, **10**, 2161.
8 D. Zhou, D. M. Gruen, L. C. Qin, T. G. McCauley and A. R. Krauss, *J. Appl. Phys.*, 1998, **84**, 1981.
9 M. N. R. Ashfold, P. W. May, J. R. Petherbridge, K. N. Rosser, J. A. Smith, Y. A. Mankelevich and N. V. Suetin, *Phys. Chem. Chem. Phys.*, 2001, **3**, 3471.
10 P. W. May and Y. A. Mankelevich, *J. Appl. Phys.*, 2006, **100**, 024301.
11 P. W. May and Y. A. Mankelevich, *J. Phys. Chem. C*, 2008, **112**, 12432.
12 C. S. Wang, H. C. Chen, H. F. Cheng and I. N. Lin, *J. Appl. Phys.*, 2010, **107**, 034304.
13 Z. Sun, J. R. Shi, B. K. Tay and S. P. Lau, *Diamond Relat. Mater.*, 2000, **9**, 1979.
14 A. C. Ferrari and J. Robertson, *Phys. Rev. B: Condens. Matter*, 2001, **63**, 121405.
15 A. C. Ferrari and J. Robertson, *Phys. Rev. B: Condens. Matter*, 2000, **61**, 14095.
16 J. Michler, Y. von Kaenel, J. Stiegler and E. Blank, *J. Appl. Phys.*, 1998, **83**, 187.
17 X. Xiao, J. Birrel, J. E. Gerbi, O. Auciello and J. A. Carlisle, *J. Appl. Phys.*, 2004, **96**, 2232.
18 A. Laikhtman, I. Gouzman, A. Hoffman, G. Comtet, L. Hellner and G. Dujardin, *J. Appl. Phys.*, 1999, **86**, 4192.
19 S. Bhattacharyya, O. Auciello, J. Birrell, J. A. Carlisle, L. A. Curtiss, A. N. Goyette, D. M. Gruen, A. R. Krauss, J. Schlueter, A. Sumant and P. Zapol, *Appl. Phys. Lett.*, 2001, **79**, 1441.
20 H. Zhou, J. Watanable, M. Miyake, A. Ogino, M. Nagatsu and R. Nhou, *Diamond Relat. Mater.*, 2007, **16**, 675.
21 J. Ma, N. Michael, R. Ashfold and Y. A. Mankelevich, *J. Appl. Phys.*, 2009, **105**, 043302.
22 G. Balestrino, M. Marinelli, E. Milani, A. Paoletti, I. Pinter, A. Tebano and P. Paroli, *Appl. Phys. Lett.*, 1993, **62**, 879.
23 M. L. Brake and T. E. Repetto, *IEEE Trans. Plasma Sci.*, 1989, **17**, 60.
24 Y. Kaga, S. Tsuge, K. Kitagawa and N. Arai, *Microchem. J.*, 1999, **63**, 34.
25 Y. Ralchenko, F. C. Jou, D. E. Kelleher, A. E. Kramida, A. Musgrove, J. Reader, W. L. Wiese and K. Olsen, *NIST Atomic Spectra Database (version 3.1.2)*. Available: http://physics.nist.gov/asd3. National Institute of Standards and Technology, Gaithersburg, MD, (2007).
26 M. Baidakova and A. Vul, *J. Phys. D: Appl. Phys.*, 2007, **40**, 6300.
27 A. M. Panich, A. I. Shames, H. M. Vieth, E. Osawa, M. Takahashi and A. Vul, *Eur. Phys. J. B*, 2006, **52**, 397.
28 P. Zapol, M. Sternberg, L. A. Curtiss, T. Frauenheim and D. M. Gruen, *Phys. Rev. B: Condens. Matter*, 2001, **65**, 045403.